

RESEARCH ARTICLE

*A three-dimensional approach to pennation angle estimation for human skeletal muscle*Dongwoon Lee^{a*}, Zhi Li^b, Qazi Zain Sohail^b, Ken Jackson^a, Eugene Fiume^a and Anne Agur^b^a*Department of Computer Science, University of Toronto, Toronto, Ontario, Canada;*^b*Department of Surgery, University of Toronto, Toronto, Ontario, Canada**(v4.1 revised February 2014)*

Pennation angle (PA) is an important property of human skeletal muscle that plays a significant role in determining the force contribution of fascicles to skeletal movement. Two-dimensional (2D) ultrasonography is the most common approach to measure PA. However, in principle, it is challenging to infer knowledge of three-dimensional (3D) architecture from 2D assessment. Furthermore, architectural complexity and variation impose more difficulties on reliable and consistent quantification of PA. Thus, the purpose of our study is to provide accurate insight into the correspondence between 2D assessment and the underlying 3D architecture. To this end, a 3D method was developed to directly quantify PA based on 3D architectural data that were acquired from cadaveric specimens through dissection and digitization. Those data were then assessed two-dimensionally by simulating ultrasound imaging. To achieve consistency over intermuscular variation, our proposed 3D method is based on the geometric analysis of fascicle attachment. Comparative results show a wide range of differences (1.1% – 47.1%) between 2D and 3D measurements. That is, ultrasound can under- or over-estimate PA, depending on architecture.

Keywords: pennation angle; line of action; ultrasonography; digitization; cadaveric specimen

1. Introduction

The physiological and mechanical functions of muscle are characterized by associated architectural parameters, such as thickness, fascicle length, pennation angle and physiological cross-sectional area (Zajac 1989). Specifically, pennation angle (PA) is an important determinant of the contribution that muscle fascicles make to the force acting along the line of action. PA is defined as the angle between the orientation of a fascicle and the attached tendon axis (i.e., the line of action) (see Figure 1(a)). For each fascicle i , its PA is simply calculated as

$$\text{PA}^i = \cos^{-1}(\text{line of action} \cdot \text{fascicle orientation}^i). \quad (1)$$

As the muscle fascicle force, \mathbf{f}_m^i , is in the direction of the fascicle orientation and the tendon force, \mathbf{f}_t , is in the direction of the line of action, their functional relation

*Corresponding author. Email: dwlee@cs.toronto.edu

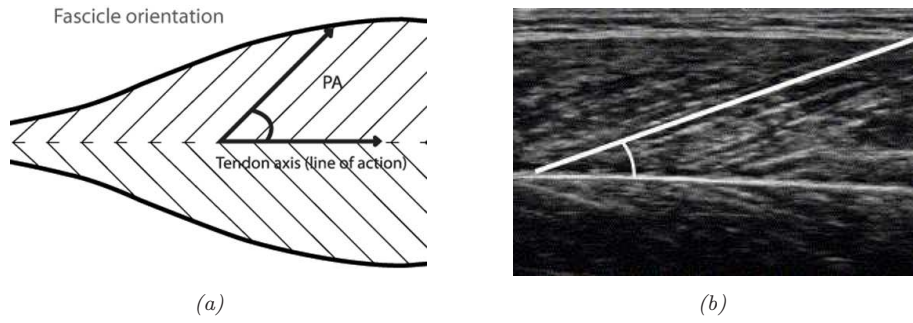


Figure 1. Pennation angle. (a) Schematic of definition. (b) Measurement on an ultrasonographic image.

is expressed as

$$\mathbf{f}_t = \sum_i \mathbf{f}_m^i \cos(\text{PA}^i). \quad (2)$$

Since fascicles have variable length and arrangement within a muscle, the associated PA differs from fascicle to fascicle (Gans and de Vree 1987; Van Donkelaar et al. 1999; Lieber and Friden 2000). For its quantification, two-dimensional (2D) ultrasonography is widely used in many clinical and biomechanical studies, because it is non-invasive, portable and applicable to dynamic measurements (e.g., muscle contraction). However, since a muscle is only assessed by 2D images, the accuracy of the measurement (up to 23% error) relies on the alignment of the imaging plane (or ultrasound probe) (Bénard et al. 2009; Rana and Wakeling 2011; Namburete et al. 2011). Since fascicles form complex and variable structures within a muscle, it is challenging to find the correct imaging plane (namely, true fascicle plane) that provides a more precise assessment of the entire three-dimensional (3D) architecture. Thus, in practice, the optimal plane is determined by satisfying the following criteria: maximum visibility of fascicles and perpendicular to the skin or deep aponeurosis. However, it is evident that individual 2D images may be subject to a limited assessment of volumetric geometry. Limited visibility and image resolution also impose further constraints on conducting detailed investigations.

In contrast to ultrasonographic assessments, the use of cadaveric specimens allow direct measurement of PA. Lieber and Friden (2000), Murray et al. (2000) and Ward et al. (2009) collected a small number of fascicles from specimen surfaces and measured PA using a hand-held goniometer or protractor. Although their direct measurements would in principle be more accurate than ultrasonographic assessments, any internal variation was not accounted for in their quantifications. On the other hand, Agur et al. (2003), Kim et al. (2007), Rosatelli et al. (2008), Ravichandiran et al. (2009) and Lee et al. (2012) conducted assessment of PA based on volumetric fascicle data that were collected throughout the muscle using dissection and digitization procedures. Those studies assumed that the line of action was aligned to the longitudinal axis of muscle (van Spronsen et al. 1987; Koolstra et al. 1989) that was approximated as an average of orientation of all fascicles. PA was then calculated as the relative angle between this axis and the fascicle orientation. However, this approximation may still fail if it is inconsistent with the underlying muscle architecture. For example, in pennate muscles, this muscle axis may not coincide with the tendon axis, because fascicles run parallel to one another, but they are variably oblique to the attached tendon axis (see Figure 2). Therefore, for consistent quantification, PA must be estimated with respect to the tendon axis. Digitizing tendons may be an immediate solution for this

problem, but certain types of tendons (e.g., intramuscular or aponeurotic tendon) may have irregular shapes and arrangements that make reconstruction challenging.

Diffusion tensor imaging (DTI) is an emerging method to investigate and visualize internal muscle architecture. Since DTI is non-invasive method, it enables *in vivo* quantification of PA throughout the volume without any tissue damage (Levin et al. 2011; Froeling et al. 2012; Schenk et al. 2013). However, it still needs to overcome some limitations related to lower signal-to-noise ratio (SNR) and difficulties in differentiating between other connective tissues.

The purpose of our study is to provide insight into the correspondence between underlying 3D architecture and 2D assessment. To this end, a 3D method was developed to directly quantify PA based on 3D architectural data (Lee et al. 2012). Those data were then assessed two-dimensionally by simulating ultrasound imaging. Using anatomically defined reference frames, region specific variation of PA within a muscle was investigated.



Figure 2. Problematic line of action estimation. Average orientation of fascicles is apparently oblique to the patellar tendon, the axis of which is directed horizontally in the given configuration.

2. Methods

Our study is based on cadaveric specimen data obtained through serial dissection and digitization procedures. Fascicles were collected and geometrically reconstructed to represent the muscle architecture. Based on the reconstructed architecture, the geometric arrangement of fascicle attachments was used to estimate PA. A reference coordinate frame was determined to evaluate region-specific variation of PA and also used to initialize the imaging plane for simulated ultrasound scans.

2.1 Data acquisition for muscle specimens

Our experimental data are acquired from a variety of muscles including two lower extremity muscles — abductor hallucis (ABH) and vastus medialis (VM) — and sixteen upper extremity muscles — anconeus (ANC), abductor pollicis longus (APL), brachialis (BR), extensor carpi radialis bevis (ECRB), extensor carpi radialis longus (ECRL), extensor carpi ulnaris (ECU), extensor digitorum (ED), extensor digitorum (EDM), extensor indicis (EI), extensor pollicis brevis (EPB), extensor pollicis longus (EPL), flexor carpi ulnaris (FCU), pectoralis major (PM), pronator teres (PT), pronator quadratus (PQ) and supraspinatus (SS). Muscle

specimens with visible abnormalities, such as muscle atrophy, fat infiltration or surgery, were excluded from the data acquisition. During dissection and digitization, associated joints were stabilized into anatomical position with metal plates and screws. Fascicles were sequentially dissected and digitized from superficial to deep throughout the muscle volume. Measurement can be taken and recorded using various three-dimensional digitizers (Dumas et al. 1988; Poelstra et al. 2000; Agur et al. 2003). Our study used a MicroScribe G2 digitizer with 0.23 mm accuracy to trace trajectories of fascicles with sampled points. Digitized fascicles were removed, exposing the underlying fascicles about 1 – 2 mm deeper. To identify fascicles accurately, a surgical microscope was used throughout the dissection and digitization process.¹ Manual identification and digitization of landmarks on specimens may be susceptible to measurement error. In a previous study, Agur et al. (2000) reported that the measurement error was small; intra-rater reliability was 0.12 – 0.70 mm ($p > 0.05$) and inter-rater reliability was 0.15 – 0.32 mm ($p > 0.05$).

2.2 Orientation of fascicles

Using the digitized points, each fascicle is first approximated by a smooth piecewise cubic spline, $\mathbf{p}(u) = (x(u), y(u), z(u))$, where $u \in [0, 1]$. The orientation of a fascicle is represented by a series of tangent vectors, $\mathbf{p}'(u) = (x'(u), y'(u), z'(u))$, along the curves (See Figure 3).

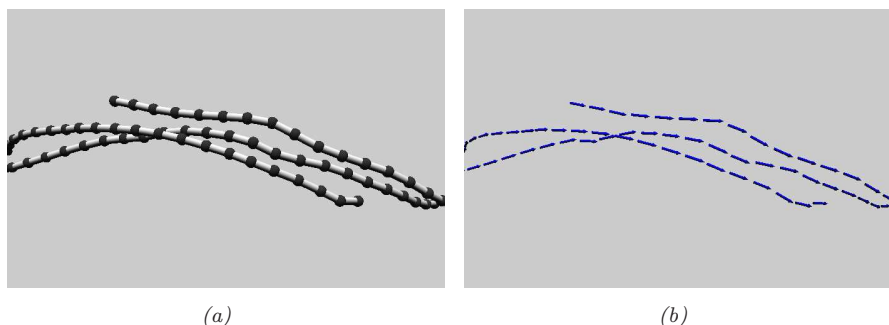


Figure 3. Representation of fascicles. (a) Spline curves and resampled points, \mathbf{p} . (b) Tangents, \mathbf{p}' , evaluated along the curves.

Using an arc-length parameterization, fascicle points are redistributed (i.e., resampled) to make the curve representation uniform (Lee et al. 2012). This redistribution is presumed to be reasonably accurate because we use a cubic Catmull-Rom spline and it is guaranteed to interpolate (i.e., to pass through) all the original digitized points. As reconstructed spline curves are clamped at their ends (i.e., tendinous attachments), tangent vectors at these points must be approximated from neighboring points, using formulas such as $\mathbf{t}(0) = \mathbf{p}'(0) \approx (\mathbf{p}(u_1) - \mathbf{p}(u_0))/(u_1 - u_0)$ and $\mathbf{t}(1) = \mathbf{p}'(1) \approx (\mathbf{p}(u_n) - \mathbf{p}(u_{n-1}))/ (u_n - u_{n-1})$. To determine proximal and distal orientation, previous studies (Ravichandiran et al. 2009; Lee et al. 2012) simply chose tangent vectors evaluated at the end points (i.e., approximations to $\mathbf{p}'(0)$ and $\mathbf{p}'(1)$). However, the positions of tendinous attachments may be slightly perturbed due to errors that may occur in the dissection and digitization procedure. This may affect the angular measurement in (1). For more reliable quantification, we take an average of the tangent fields evaluated over a local area close to these attachments.

¹Ethics approval was obtained from the Research Ethics Board at the University of Toronto (Protocol Reference Number: 27210).

More specifically, for each fascicle i , the averaged tangent vectors for proximal, $\overline{\mathbf{t}}_p^i$, and distal, $\overline{\mathbf{t}}_d^i$, orientations are calculated as

$$\overline{\mathbf{t}}_p^i = \frac{1}{n_p} \sum_{u=0}^{u_p} \mathbf{t}^i(u) \quad (3)$$

$$\overline{\mathbf{t}}_d^i = \frac{1}{n_d} \sum_{u=u_d}^1 \mathbf{t}^i(u) \quad (4)$$

where $\mathbf{t}^i(u)$ is the tangent vector for fascicle i defined at the point $\mathbf{p}(u)$, n_p and n_d are the number of points in the local proximal and distal regions, respectively, and $u \in [0, \dots, u_p, \dots, u_d, \dots, 1]$. In practice, we choose $0.15 - 0.2$ for u_p and $0.8 - 0.85$ for u_d , whence approximately 15 – 20% of the entire fascicle length is included in each of the proximal and distal regions.

2.3 Line of action

The line of action of a muscle can be approximated by the long axis of the internal tendon onto which the fascicles attach. For non-pennate muscles, such as fusiform and parallel muscles, the average direction of collective forces exerted by all fascicles is parallel, or nearly parallel, to the axis of the attached tendon. Thus, the line of action can be approximated as (Ravichandiran et al. 2009; Lee et al. 2012)

$$\begin{aligned} \text{line of action}_p &= \frac{1}{n} \sum_{i=1}^n \overline{\mathbf{t}}_p^i \\ \text{line of action}_d &= \frac{1}{n} \sum_{i=1}^n \overline{\mathbf{t}}_d^i \end{aligned} \quad (5)$$

where n is the number of fascicles. This approach, based on Equation (5), is conceptually similar to the method described in (Koolstra et al. 1989): the estimated centre line corresponds to an average direction of all fascicles (see Figure 4). However, equation (5) may be inappropriate for pennate muscles, because fascicles are often oblique, rather than parallel, to attached tendons. Thus, the averaged direction of fascicles may produce a poor estimate of the line of action (see Figure 2). Digitized tendons or aponeuroses could be used to determine the line of action, but, compared to fascicle data, they are often observed to be irregular and non-homogeneous in terms of arrangement or shape. Thus, the fascicle data may be more straightforward and simpler to deal with computationally.

From our specimen data, we observe that the geometric arrangement of fascicle attachments reveals the directionality of the tendons. For instance, in pennate muscles, tendinous attachments are linearly arranged, whereas in non-pennate muscle, they are arranged in more diverse patterns. To be more specific, for pennate muscles, the distribution of the attachment points is approximately represented as a long and thin ellipsoid, the principal axis of which roughly matches the tendon axis. The least square regression method can be used to find this axis:

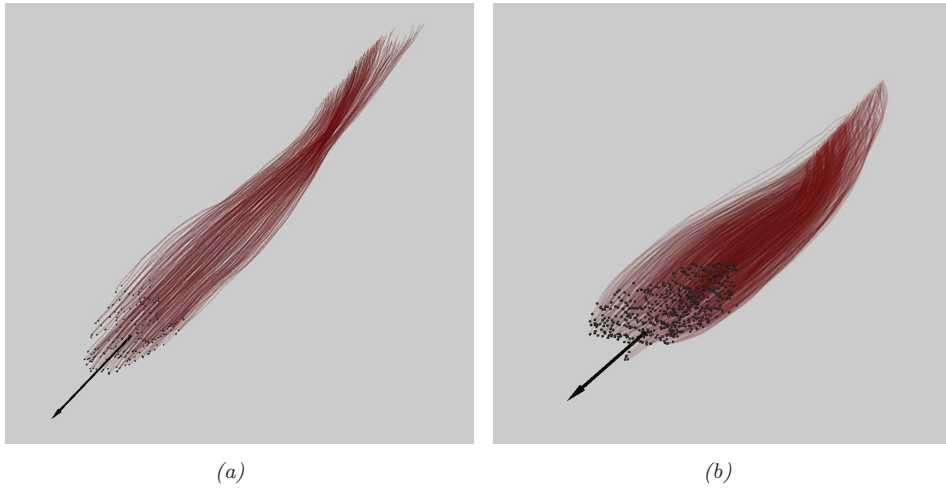


Figure 4. Estimated line of action (black arrow) and distal attachments (black dots) of fascicles (red) for fusiform muscle. (a) Brachioradialis. (b) Extensor carpi radialis longus.

$$\min_{\beta_1 \beta_2} \sum_i \|S(\mathbf{p}_i) - \beta_1 t_i - \beta_0\|^2 \quad (6)$$

where $S(\mathbf{p})$ denotes the attachment points and $\beta_1 t + \beta_0$ is the linear regression model to fit (β_1 : slope, β_0 : y-intercept, t : parametric variable). The vector β_1 is the estimated principal axis for the line of action (see Figure 5).

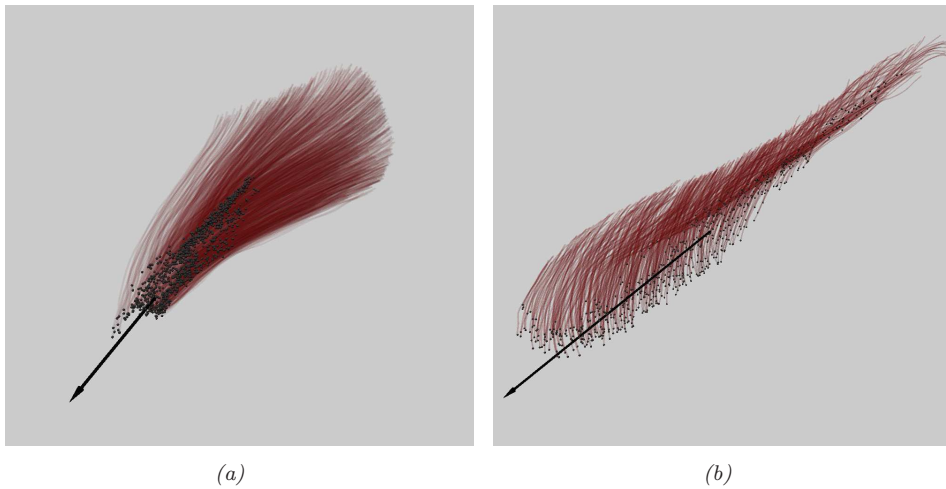


Figure 5. Estimated line of action (black arrow) and distal attachments (black dots) of fascicles (red) for pennate muscle. (a) Supraspinatus. (b) Vastus medialis.

2.4 Pennate and non-pennate muscles

Depending on pennation, the line of action in (1) is determined by using either (5) or (6). For reliable quantification of PA, the method for determining the line of action must be chosen consistently. To this end, recall that attachments of fascicles are arranged linearly in pennate muscle, but are more complex in non-pennate muscle. To utilize this characteristic in determining the type of muscle, we evaluate the quality of the fit in (6) by considering

$$r^2 = 1 - \frac{\sum_{i=1}^n \|S(\mathbf{p}_i) - \beta_1 t_i - \beta_0\|^2}{\sum_{i=1}^n \|S(\mathbf{p}_i) - \overline{S(\mathbf{p})}\|^2} \quad (7)$$

where $\overline{S(\mathbf{p})} = \frac{1}{n} \sum_{i=1}^n S(\mathbf{p}_i)$ and n is the number of attachment points. Here, $r^2 = 1.0$ indicates a perfect fit of our regression model, while $r^2 = 0.0$ is associated with the poorest fit. Because of the linearity of their attachment arrangement, pennate muscles have high values of r^2 , whereas non-pennate muscles have lower values of r^2 . Based on this difference, a threshold for the r^2 value can be chosen to classify muscles as either pennate or non-pennate. However, some pennate muscles, which are directly attached to bones without any external tendons, may need to be classified differently. In such cases, the line of action is approximated as the average orientation of fascicles using (5) instead (see Figure 6). Attachment types (i.e., tendinous or bony attachment) can be determined during the dissection and digitization process.

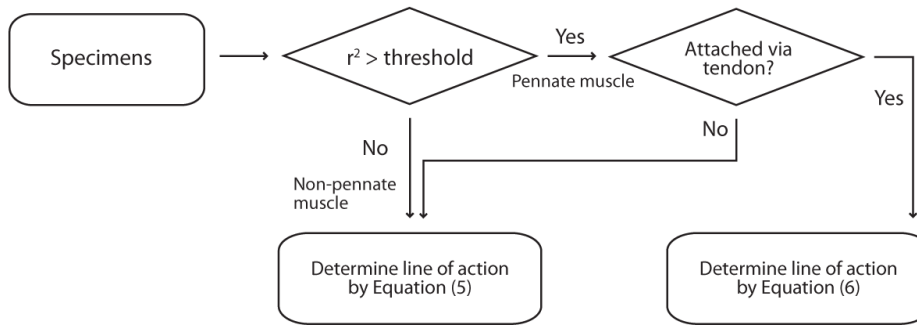


Figure 6. Flow chart for our method to determine the line of action.

2.5 Anatomical reference frame

A reference coordinate frame is determined for our further analysis of the correlation between the PA distribution and the fascicles' anatomical positions within the muscle volume. To this end, a three-dimensional Cartesian coordinate system is formed by the three orthogonal axes that originate from the geometric centre of the muscle and correspond to the standard anatomical directions: proximo-distal, superficial-deep and latero-medial (or anterior-posterior) (see Figure 7). It is common practice to undertake radiological assessment with respect to anatomical planes rather than other coordinate (or axis) systems. For the results to be comparable to clinical findings, we use anatomical planes as the reference frame throughout this paper.

The estimated line of action (described in Section 2.3) is used to represent the proximo-distal axis. Subsequently, the cross-section, π_C , is defined as the plane that is transverse to the proximo-distal axis and located at the origin of the coordinate frame (see Figure 7(b)). The intersection of π_C and the fascicles yields a two-dimensional point-set, $\{S(\mathbf{p}_c)\}$. Many superficial muscles have elliptical cross-sections, the longer and shorter axes of which approximately correspond to the latero-medial and the superficial-deep axes, respectively (See Figure 7(c)). These axes can be effectively estimated by a principal component analysis (PCA): the eigenvector associated with the larger eigenvalue approximates the major

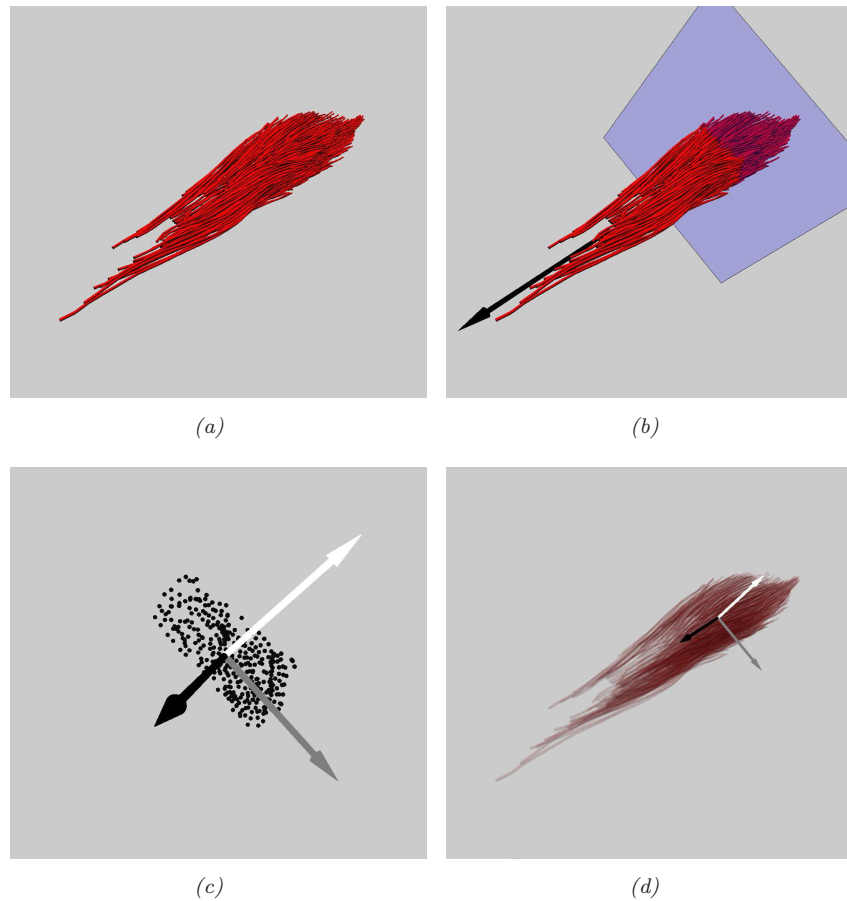


Figure 7. Anatomical reference frame. (a) Fascicles of extensor digitorum muscle. (b) Illustration of the line of action, shown as the black arrow in the distal region, and the corresponding cross-section, π_C , shown as the purple plane. (c) Intersection points of π_C with the fascicles and the estimated anatomical directions, superficial-deep (white arrow) and the medial-lateral (gray arrow). (d) Reference coordinate frame shown with the fascicles.

axis of the ellipse whereas the eigenvector associated with the smaller eigenvalue represents its minor axis. In the case of muscles that have circular cross-sections (e.g., ECRL), the axes determination may be inconsistent, as those eigenvectors may not coincide with the corresponding anatomical axes. Consequently, manual adjustment may be required. With regard to the proximo-distal axis, all distal attachments of the fascicles are projected onto this axis and their relative positions are used to evaluate correlation. Regarding the latero-medial and superficial-deep axes, the geometric deviations of all fascicles from the centre of the muscle are calculated and then assessed in relation to the axes.

If a muscle is subdivided into multiple parts (heads), based on attachment site and spatial arrangement of fascicles, our analysis was conducted separately for each part using its own reference system and geometric centre.

2.6 Simulated ultrasound assessment

Two-dimensional (2D) ultrasound assessment is simulated by projecting fascicles onto the imaging plane, which is determined by the linear combination of two reference axes (see Figure 8). The longitudinal plane is defined by either the proximo-distal and the latero-medial axes or the proximo-distal and superficial-deep axes. The transverse plane is defined by the latero-medial and superficial-deep axes.

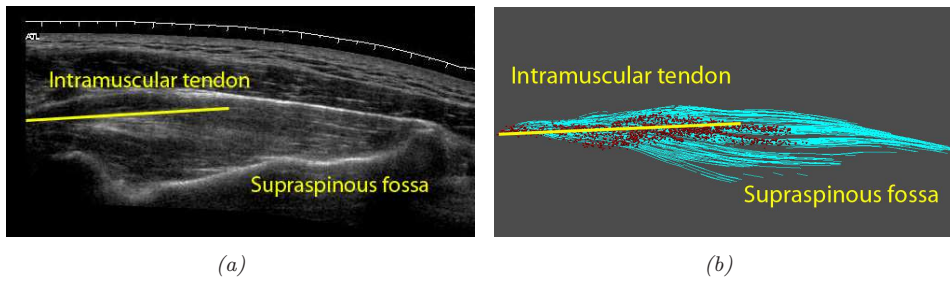


Figure 8. Mid-longitudinal images of Supraspinatus: (a) living subject by ultrasound. (b) cadaveric specimen (digitized fascicle data) by simulated ultrasound.

Translating and rotating these planes imitates the alignment control of the ultrasound probe. To create a 2D image, viewable fascicles are identified by evaluating their proximity to the imaging plane and then they are projected onto that plane. To be comparable to an ultrasound scan, the simulated imaging plane is initially positioned at the geometric centre of the muscle and aligned to the mid-longitudinal plane. Then, the position and orientation of the plane are adjusted by up to ± 10 mm and $\pm 15^\circ$, respectively, to maximize the number of viewable fascicles. PA is then calculated based on the projected fascicle image using the projected 2D fascicles and the line of action. In some cases, only the middle portion of a fascicle is visible in the projected image. In such cases, it may be inaccurate to estimate the fascicle’s tangent vector at the attachments points by extrapolation. Thus, in practice, when calculating PA, we use only the projected fascicles that have a viewable portion that includes at least 15 – 20% of the proximal and distal regions (similar to Section 2.2).

3. Results

Our PA estimation results for 18 muscles, using both 2D and 3D methods, are given in Table 1. The 2D method is based on the simulated ultrasound imaging method described in Section 2.6. Our new 3D method is described in Sections 2.1–2.5. The PA estimation results are also presented graphically in Figures 9, 10 and 11.

Muscle	N (N_{2D})	Pattern	r^2	PA_{3D}	PA_{2D}
ABH	396 (136)	pennate	0.98	18.9 ± 8.9 (0.7 – 52.1)	13.8 ± 9.6 (0.4 – 46.5)
ANC	728 (64)	non-pennate	0.96	16.8 ± 12.3 (0.5 – 78.8)	10.2 ± 6.3 (0.9 – 29.5)
APL	620 (184)	pennate	0.98	13.1 ± 5.6 (0.6 – 40.2)	11.3 ± 7.7 (0.1 – 37.0)
BR	182 (24)	non-pennate	0.67	3.1 ± 2.2 (0.1 – 10.8)	4.3 ± 3.7 (0.1 – 15.6)
ECRB	630 (306)	pennate	0.93	14.2 ± 4.9 (1.8 – 35.1)	8.2 ± 6.1 (2.5 – 54.3)
ECRL	629 (84)	non-pennate	0.82	11.9 ± 5.1 (1.0 – 33.4)	12.8 ± 7.8 (0.2 – 31.6)
ECU	449 (126)	pennate	0.99	6.4 ± 2.9 (0.4 – 19.0)	5.5 ± 4.0 (0.1 – 17.7)
ED	460 (89)	pennate	0.97	9.3 ± 3.5 (0.3 – 22.1)	9.2 ± 5.9 (0.4 – 29.8)
EDM	158 (82)	pennate	0.99	5.6 ± 2.5 (0.4 – 10.7)	4.8 ± 3.5 (0.0 – 22.4)
EI	176 (89)	pennate	0.98	9.6 ± 4.4 (0.6 – 21.9)	7.6 ± 6.2 (0.2 – 27.1)
EPB	155 (63)	pennate	0.96	22.9 ± 8.8 (9.5 – 49.9)	21.5 ± 17.9 (0.6 – 85.0)
EPL	201 (65)	pennate	0.99	6.4 ± 3.0 (0.8 – 15.8)	5.2 ± 3.5 (0.2 – 17.8)
FCU	1047 (442)	pennate	0.99	15.4 ± 6.9 (0.5 – 37.6)	10.1 ± 7.6 (0.1 – 42.2)
PM	792 (64)	non-pennate	0.78	13.6 ± 10.2 (0.2 – 41.3)	7.2 ± 5.1 (0.2 – 20.9)
PQ	910 (78)	non-pennate	0.69	19.6 ± 10.3 (2.9 – 59.6)	12.3 ± 13.7 (0.1 – 76.8)
PT	1218 (313)	pennate	0.98	15.8 ± 7.0 (0.3 – 43.1)	12.2 ± 8.3 (0.1 – 44.1)
SS	1750 (723)	pennate	0.92	16.5 ± 9.5 (0.4 – 43.9)	13.1 ± 3.6 (0.9 – 43.2)
VM	703 (370)	pennate	0.97	34.5 ± 15.7 (2.6 – 70.0)	30.4 ± 13.6 (1.6 – 83.2)

Table 1. Estimation of PA at distal attachments. N is the total number of digitized fascicles. N_{2D} is the number of projected fascicles in the imaging plane. r^2 is the coefficient of determination of linearity in (7). PA_{3D} and PA_{2D} are the estimated PA using the 3D method and the 2D method, respectively. The value of PA (in degrees) is given as ‘the mean \pm the standard deviation (min-max)’.

3.1 Pennate and non-pennate muscles

The linearity of the geometric arrangement of the distal attachments is evaluated using (7). Quantitatively, a muscle is considered to be pennate when the distal attachment exhibits stronger linearity (i.e., r^2 is greater than 0.9), whereas, in contrast, non-pennate (i.e., fusiform and parallel) muscles exhibit markedly weaker linearity (i.e., r^2 is less than 0.9). Thus, we use 0.9 as the threshold in deciding to classify muscle as pennate or non-pennate (see Figure 6). However, there exist exceptional cases that may need to be dealt with differently, such as ANC. Although the distal attachment for ANC muscle exhibits a strong linear arrangement ($r^2 = 0.962$), the estimated axis may not represent its tendinous axis, since the ANC muscle is attached directly to the ulna without an external tendon. Consequently, this estimated axis may coincide with the longitudinal axis of the bone. In such cases for which a muscle is attached directly to a bone, the line of action is approximated as an average orientation of fascicles using (5) instead of (6).

Fan-shaped muscles (ANC, PM and PQ) have substantial variation in their PA, whereas fusiform or parallel muscles (BR, ECRL) have a relatively small range of PA values. In fan-shaped muscles, fascicles are spread over a broad area and converge into a narrow attachment site. Their PA varies considerably from the fascicles located farthest from the central axis (78.81° in ANC) to ones located closest to this axis (0.48° in ANC). In pennate muscles, fascicles are inserted more obliquely at the distal end of the tendon, whereas they are nearly parallel to the axis of the tendon at the proximal end.

3.2 Region-specific variation of PA

To effectively visualize local variation of PA throughout a muscle, its distribution is normalized and mapped onto a color gradient ranging from red (PA_{min}) to blue (PA_{max}). The correlation between region and PA is mathematically quantified by associating the geometric location of the fascicle with the three anatomical axes as described in Section 2.5. With respect to these axes, the distribution of PA is depicted in plots and the observed correlations are expressed using fitted polynomial functions. Our results demonstrate that the correlation patterns may differ from muscle to muscle and furthermore that one axis may have a stronger correlation than another. In relation to the anatomical axes, PA changes either monotonically (e.g., decreasing or increasing) or non-monotonically (e.g., decreasing and then increasing). In most cases, these patterns are well-fitted by either a linear or a quadratic function.

Among the muscles we studied, the pennate muscles are commonly observed to have increasing PA in the proximo-distal direction. This correlation is stronger for unipennate muscles (e.g., EPB and VM) than for other types of muscles, because these unipennate muscles have a relatively simple architectural pattern in that the fascicles are attached to only one side of the tendon (see Figure 9). The correlation with the proximo-distal direction rarely occurs for non-pennate muscles (e.g., BR and ECRL). Instead, these muscles are observed to have a changing pattern of PA in the transverse direction, such as lateral to medial or superficial to deep (see Figure 10). Similarly, in bipennate muscles, PA distribution may be characterized with respect to the latero-medial direction, because, in those muscles, the geometric deviation of fascicles from the line of action (i.e., extramuscular tendon for non-pennate muscles and intramuscular tendon for bipennate muscles) can be quantified

in the transverse direction, which is proportional to their PA. Fascicle arrangement may be nearly symmetric (e.g., ECRB) or asymmetric (e.g., APL) in relation to the tendon, which leads to either non-monotonic or monotonic PA distribution (see Figure 11).

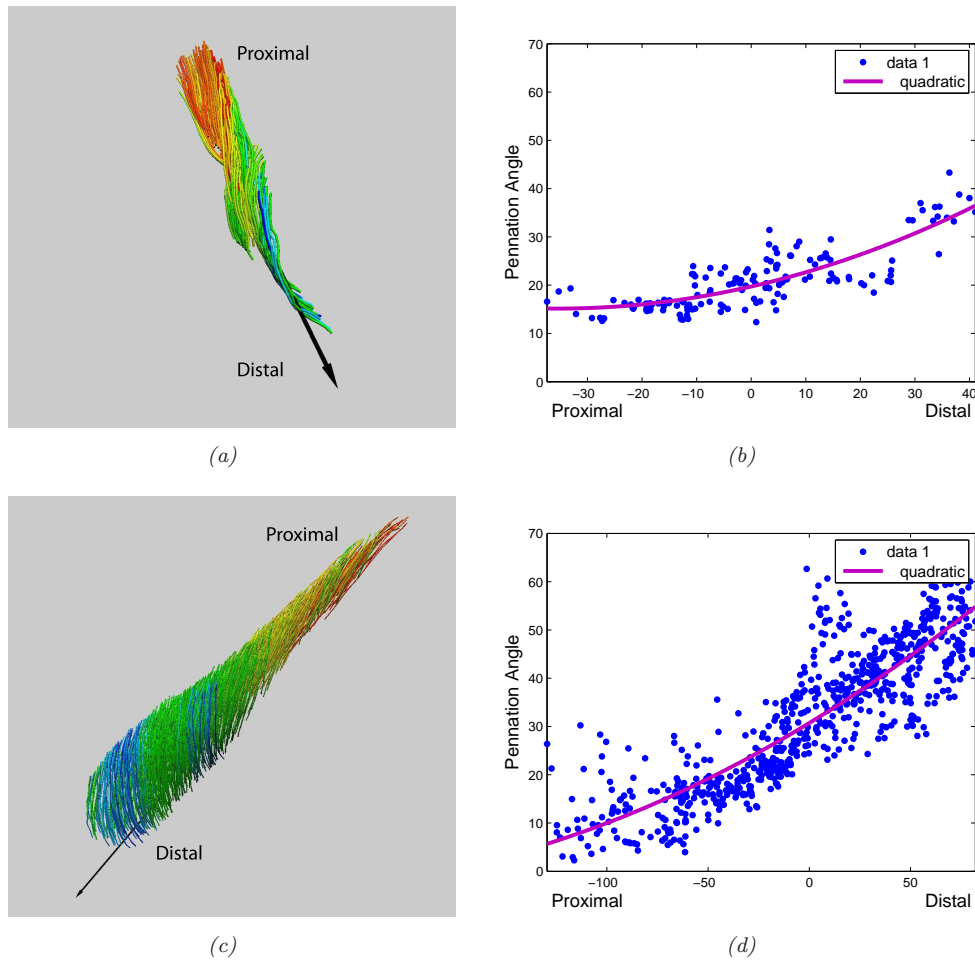


Figure 9. PA variation and its correlation with the proximal-distal direction for unipennate muscles. (a) Entire color field of PA for EPB. (b) PA distribution and its fitted model: $y = 0.0036373x^2 + 0.25795x + 19.721$. (c) Entire color field of PA for VM. (d) PA distribution and its fitted model: $y = 0.00047506x^2 + 0.25476x + 30.719$.

3.3 Comparison of 3D and 2D estimation of PA

The difference between the estimated PA computed by the 3D and 2D methods varies substantially (1.1% – 47.1%) and depends on the architectural pattern of the muscle. The 2D method yields a smaller estimation of PA than does the 3D method for all but fusiform muscles (BR and ECRL). A significant difference of PA (37.2% – 47.1%) occurs for fan-shaped muscles (ANC, PM and PQ). For bipennate muscles, the difference of PA varies widely (1.1% – 42.2%), whereas for unipennate muscles (EPB and VM), the difference is smaller (6.1% – 11.9%).

Unlike the 3D method, the 2D method does not take all fascicles into account when estimating PA. More specifically, in the 2D method, only a subset of fascicles (8.1% – 52.6%) that intersect the imaging plane contribute to PA estimation. Furthermore, 2D projection may introduce an angular error. Ultimately, this

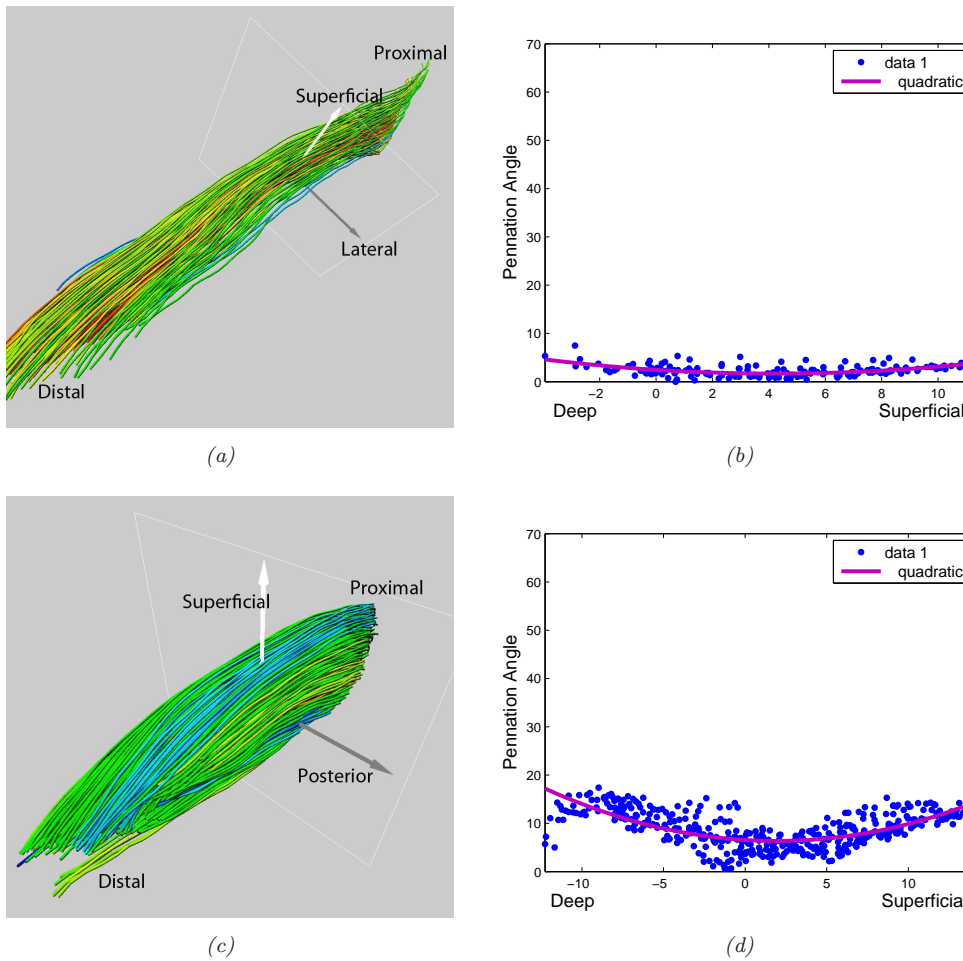


Figure 10. PA variation and its correlation with the superficial-deep direction for fusiform muscles. (a) Entire color field of PA for BR. (b) PA distribution and its fitted model: $y = 0.043905x^2 - 0.37168x + 2.4642$. (c) Entire color field of PA for ECRL. (d) PA distribution and its fitted model: $y = 0.05396x^2 - 0.20736x + 6.5558$.

comparative result is mainly due to how closely the 2D distribution of projected fascicles approximates the entire architecture of the muscle. For the 2D method, the mid-longitudinal imaging plane is defined by the proximo-distal and superficial-deep axes. Among our studied muscles, fusiform muscles and unipennate muscles have substantial variation of PA along either the proximo-distal or superficial-deep axis. Since the imaging plane contains both axes, it is likely that the 2D distribution of fascicles shows a similar variation pattern to what is observed in 3D. As fascicles are located farther from the plane, some become more parallel (e.g., BR and ECRL) while others remain oblique to the tendon axis (e.g., EPB and VM). Thus, their PA is close to zero or still considerable, respectively. Since those fascicles do not appear in 2D images, the resulting average PA using the 2D method can be slightly larger or smaller than the PA computed by the 3D method. Fan-shaped muscles and some bipennate muscles (e.g., ECRB and FCU) have a stronger pattern of fascicle angulation along the latero-medial axis than along the other axes. This is rarely captured in the imaging plane. In such cases, the 2D method yields much smaller PA estimates than does the 3D method.

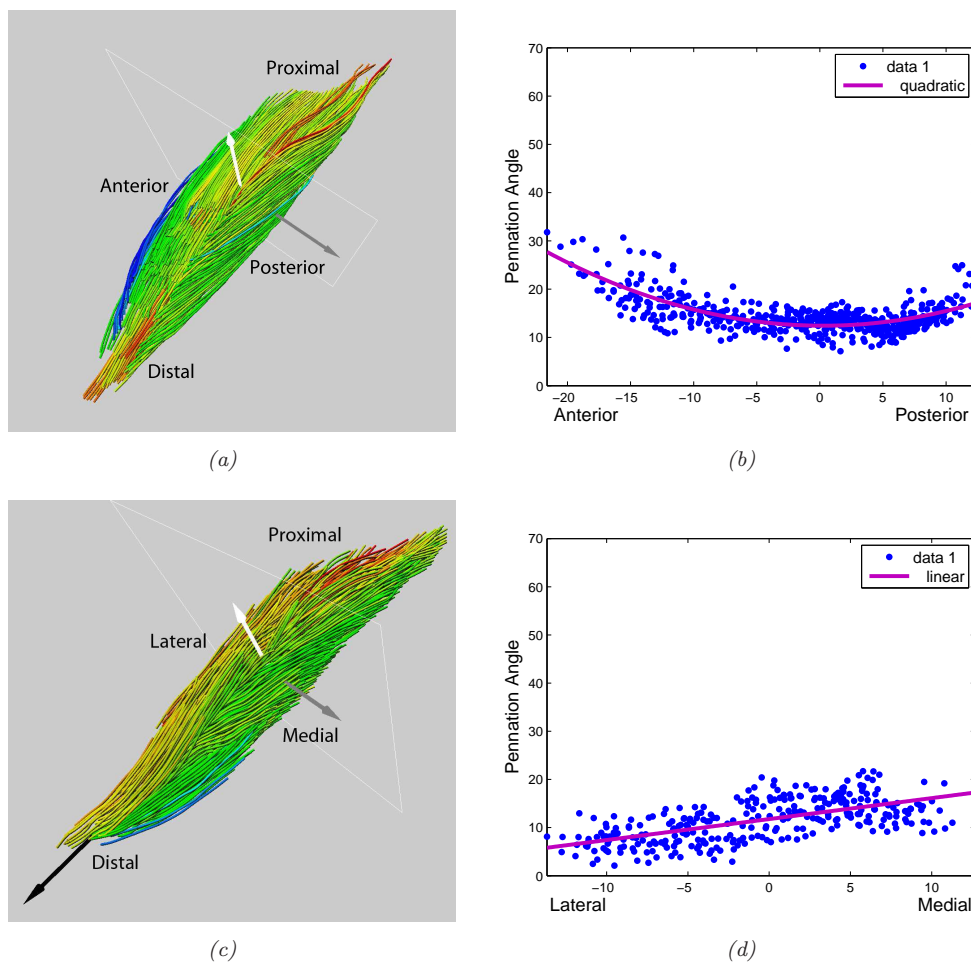


Figure 11. PA variation and its correlation with the medial to lateral (or anterior to posterior) direction for bipennate muscles. (a) Entire color field of PA for ECRB. (b) PA distribution and its fitted model: $y = 0.031945 x^2 - 0.015641 x + 12.433$. (c) Entire color field of PA for APL. (d) PA distribution and its fitted model: $y = 0.43524 x + 11.766$.

4. Discussion

PA is an important architectural parameter used to characterize muscle functions. Ultrasonography is the most commonly used approach to measure PA. It provides 2D assessment based on a hand-held probe. However, 2D assessment is subject to some uncertainty and ambiguity, which may result in under- or over-estimation of PA. This may lead to critical problems in both computational studies and diagnostic treatments. Thus, when using ultrasonography, it is important to find the optimal imaging plane so that PA can be reliably quantified. To do so, requires a good understanding of 3D muscle architecture and the corresponding 2D assessment of the imaging scan. To this end, our study focuses on developing both 3D and 2D approaches to quantifying PA. Our proposed 3D approach directly quantifies PA from digitized fascicle data. The geometric analysis of fascicle attachment permits it to handle architectural variation consistently. Our volumetric data allows us to conduct detailed investigations of PA variation that may be characterized with respect to the anatomical axes. The 2D approach, based on simulated ultrasound imaging, is used to compare 3D and 2D measurements. Their difference can be used to assess the resemblance between 3D arrangement of fascicles in space and their projected 2D arrangement.

Our 3D method can be directly applied to fascicle data that are obtained by DTI method (Levin et al. 2011; Froeling et al. 2012). However, since our study is based on cadaveric specimen data that were collected invasively, it may not be directly applicable to *in vivo* quantification based on ultrasonography. Nevertheless, it could provide insight into determining a good scanning plane with respect to the underlying muscle architecture. For instance, it is observed that some bipennate muscles (e.g., ECRB and FCU) and fan-shaped muscles have strongly varying PA along the latero-medial axis. If the imaging plane is aligned to include this axis, 2D measurements become more compatible with 3D measurements. Our study also suggests that multiple scans should be performed at different positions for muscles having multiple bellies or distinct regions that may have functional differences.

Although our study provides improved capability for PA estimation, there are some limitations to overcome. First, our comparative study should be extended to include true ultrasonographic assessment, not just simulated results. Second, our analysis does not include the inter-muscular variation of PA. A study of such variation would require more specimens. Last, we hope to extend our 3D method to a variety of *in vivo* applications, including dynamic applications. To this end, we plan to investigate the integration of 3D architectural data and *in vivo* measurements.

Acknowledgement

This research was supported in part by the Natural Sciences and Engineering Research Council (NSERC) of Canada and the GRAND NCE of Canada.

References

- Agur A, Mahoney M, Marley K, Ng-Thow-Hing V, Fiume E. 2000. Reliability of modeling human skeletal muscle architecture using a 3D-X Microscribe digitizer. In: *Plastic Surgery Research Council 45th Annual Meeting, WA, USA, May 17-28, 2000*.
- Agur A, Ng-Thow-Hing V, Ball K, Fiume E, McKee N. 2003. Documentation and three-dimensional modelling of human soleus muscle architecture. *Clinical Anatomy* 16(4):285–293.
- Bénard M, Becher J, Harlaar J, Huijing P, Jaspers R. 2009. Anatomical information is needed in ultrasound imaging of muscle to avoid potentially substantial errors in measurement of muscle geometry. *Muscle Nerve* 39(5):652–665.
- Dumas GA, J. PM, Roy B, Gagnon M, Jovanovic M. 1988. A three-dimensional digitization method to measure trunk muscle lines of action. *Spine* 13:532–541.
- Froeling M, Nederveen A, Heijtel D, Lataster A, Bos C, Nicolay K, Maas M, Drost M, Strijkers G. 2012. Diffusion-tensor MRI reveals the complex muscle architecture of the human forearm. *Journal of Magnetic Resonance Imaging* 36:237–248.
- Gans C, deVree F. 1987. Functional bases of fiber length and angulation in muscle. *Journal of Morphology* 192:63–85.
- Kim S, Boynton E, Ravichandiran K, Fung L, Bleakney R, Agur A. 2007. Three-dimensional study of the musculotendinous architecture of supraspinatus and its functional correlations. *Clinical Anatomy* 20:648–655.
- Koolstra J, van Eijden T, Weijs W. 1989. An iterative procedure to estimate muscle lines of action in vivo. *Journal of Biomechanics* 22:911–920.
- Lee D, Ravichandiran K, Jackson K, Fiume E, Agur A. 2012. Robust estimation of physiological cross-sectional area and geometric reconstruction for human skeletal muscle. *Journal of Biomechanics* 45(8):1507–1513.
- Levin DI, Gilles B, Madler B, Pai DK. 2011. Extracting skeletal muscle fiber fields from noisy diffusion tensor data. *Medical Image Analysis* 15:340–353.
- Lieber R, Friden J. 2000. Functional and clinical significance of skeletal muscle architecture. *Muscle Nerve* 23:1647–1666.
- Murray WM, Buchanan TS, Delp SL. 2000. The isometric functional capacity of muscles that cross the elbow. *Journal of Biomechanics* 33:943–952.
- Namburete AI, Rana M, Wakeling JM. 2011. Computational methods for quantifying in vivo muscle fascicle curvature from ultrasound images. *Journal of Biomechanics* 44:2538–2543.

- Poelstra KA, Eijkelkamp MF, Veldhuizen AG. 2000. The geometry of the human paraspinal muscles with the aid of three-dimensional computed tomography scans and 3-Space Isotrak. *Spine* 25:2176–2179.
- Rana M, Wakeling J. 2011. In-vivo determination of 3D muscle architecture of human muscle using free hand ultrasound. *Journal of Biomechanics* 44:2129–2135.
- Ravichandiran K, Ravichandiran M, Oliver M, Singh K, McKee N, Agur A. 2009. Determining physiological cross-sectional area of extensor carpi radialis longus and brevis as a whole and by regions using 3D computer muscle models created from digitized fiber bundle data. *Comput. Methods Prog. Biomed.* 95:203–212.
- Rosatelli A, Ravichandiran K, Agur A. 2008. Three-dimensional study of the musculotendinous architecture of lumbar multifidus and its functional implications. *Clinical Anatomy* 21:539–546.
- Schenk P, Siebert T, Hiepe P, Gullmar D, Reichenbach JR, Wick C, Blickhan R, Böl M. 2013. Determination of three-dimensional muscle architectures: validation of the DTI-based fiber tractography method by manual digitization. *Journal of Anatomy* 223:61–68.
- Van Donkelaar C, Kretzers L, Bovendeerd P, Lataster L, Nicolay K, Janssen J, Drost M. 1999. Diffusion tensor imaging in biomechanical studies of skeletal muscle function. *Journal of Anatomy* 194:79–88.
- van Spronsen PH, Valk J, Weijts WA, Prahl-Andersen B. 1987. Analysis of masticatory muscle orientation in adults by means of MRI. *Acta Anatomica* 130:96–97.
- Ward S, Kim C, Eng C, Gottschalk L, Tomiya A, Garfin S, Lieber R. 2009. Architectural analysis and intraoperative measurements demonstrate the unique design of the multifidus muscle for lumbar spine stability. *J Bone Joint Surg Am* 91:176–185.
- Zajac F. 1989. Muscle and tendon: properties, models, scaling, and application to biomechanics and motor control. *Critical Reviews in Biomedical Engineering* 17:359–411.